

## Article

# Steady-State Control of Fuel Cell Based on Boost Mode of a Dual Winding Motor

Cheng Chang, Weibin Chang, Jiangang Ma and Yafu Zhou \*

School of Automotive Engineering, Faculty of Vehicle Engineering and Mechanics, State Key Laboratory of Structural Analysis for Industrial Equipment, Dalian University of Technology, Dalian 116024, China; dlutcc@mail.dlut.edu.cn (C.C.); dluter\_cwb@mail.dlut.edu.cn (W.C.); jiangang\_ma@126.com (J.M.)

\* Correspondence: dlzyf@dlut.edu.cn; Tel.: +86-133-3223-6235

**Abstract:** In recent years, a dual winding motor drive has been proposed in the field of fuel cell vehicles due to its advantages of good performance and high robustness. This new topology and its basic control method have been widely investigated. However, the previous research has not considered the current dynamic property of a fuel cell when studying the power sharing control method, but this is an important research objective for fuel cell durability. Considering the current change principle of a fuel cell, an optimal steady-state control method based on a new dual winding motor architecture boost charging is proposed to optimize the fuel cell life. In addition, in view of the current circulation problem of the fuel cell side winding in the boost mode, a Bang-Bang-PI control algorithm with a relatively constant reference value is proposed to realize the current sharing control. On this basis, the optimized control of the output current ripple of the fuel cell is realized to ensure the steady-state of the proton exchange membrane fuel cell (PEMFC). Finally, the results show that this method can control the stability of the fuel cell efficiently.

**Keywords:** dual winding motor; input current control; fuel cell steady-state control; current circulation; fuel cell vehicle



**Citation:** Chang, C.; Chang, W.; Ma, J.; Zhou, Y. Steady-State Control of Fuel Cell Based on Boost Mode of a Dual Winding Motor. *Energies* **2021**, *14*, 4673. <https://doi.org/10.3390/en14154673>

Academic Editor: Andrea Mazza

Received: 22 June 2021

Accepted: 28 July 2021

Published: 1 August 2021

**Publisher's Note:** MDPI stays neutral with regard to jurisdictional claims in published maps and institutional affiliations.



**Copyright:** © 2021 by the authors. Licensee MDPI, Basel, Switzerland. This article is an open access article distributed under the terms and conditions of the Creative Commons Attribution (CC BY) license (<https://creativecommons.org/licenses/by/4.0/>).

## 1. Introduction

### 1.1. Background

A proton exchange membrane fuel cell (PEMFC) is a promising energy conversion device for automotive applications due to its low operation temperature, fast start-up, and high power density [1]. After continuous optimization, significant progress in the PEMFC has been made recently. However, durability and cost are still two main limitations for achieving global commercialization [2].

### 1.2. Current Variation Principle of Fuel Cell

Sudden changes in the output current can cause variations in the water content and gas content inside a PEM fuel cell, which is the driving force for extensive degradation processes, such as membrane deformation, carbon corrosion, and platinum dissolution. The main reason for these variations is a degradation in reactant concentration response for oxygen and hydrogen under a transient load. These variations cause periodic humidity cycling, which further cause swelling and shrinking of the Nafion membrane. Finally, the resultant periodic mechanical stresses decrease the membrane lifespan.

Theiler et al. investigated the correlation between the humidity cycle and fuel cell lifetime and concluded that the mechanical lifetime of the Nafion membrane decreased with a variation in the humidity level, and the lifetime appeared to be minimal when the cycling period was in the range of 50 s to 150 s [3].

Gemmen revealed that when the DC current ripple frequency was below 120 Hz, the resultant degradation of the reactant concentration response for oxygen and hydrogen had a significant impact on the fuel cell operation. He suggested that for ensuring negligible

ripple impact, DC current ripple frequencies should be above 120 Hz or should have a ripple of less than 4% [4].

In summary, the LFCR should be as low as possible (i.e., 4% of the reference value) and the current ripple should avoid the frequency range of 0.1–0.005 Hz.

### 1.3. LFCR Generation Mechanism

The current ripple on the AC side will cause contribution and superposition on the DC side due to the transient load change, pulse-width modulation strategy, and cross-coupling between the two windings, and these fluctuations could be amplified when the frequency of the DC current ripple resonates with the circuit [5]. The frequency spectrum of the pulse width modulation (PWM) switching waveform and its impact on the DC side have been widely investigated, precisely defined, and no further discussion is needed [6,7]. It should be noted that periodic DC current fluctuations caused by a PWM denote kHz-class high-frequency small-amplitude fluctuations, which have a little impact on the fuel cell Nafion membrane lifetime because the hydrogen concentration response decreases slightly in high-frequency (e.g., above 240 Hz) and low-current-density regions (e.g., below 3000 A/m<sup>2</sup>). Therefore, transient load change and cross-coupling are two main reasons for the LFCR, and they influence the fuel cell lifespan. However, this effect has been rarely researched in fuel cell-related literature.

### 1.4. Dual Winding Motor Control Methods

Considering that in the working mode of a fuel cell vehicle (FCV) the speed and torque value undergo transient changes, a sudden change in the output current of the fuel cell can be caused, which adversely affects its durability. For the conventional drivetrain of an FCV, the main DC–DC converter is adopted between the PEMFC and battery, acting as a power distributor and a voltage adapter [8].

In recent years, a new drivetrain for FCVs has been investigated to meet the increasing demands for lifespan improvement and cost reduction. Among different topologies, the dual winding motor (DWM) drive has attracted great attention due to its advantages of reduced phase current rating, low DC-link current harmonic, small torque ripples, improved efficiency, and fault-tolerance characteristics [9]. Extensive efforts have been made over the past few years. Bojoi et al. [10] presented an FCV drivetrain topology based on the dual three-phase induction motor drive system and proposed a novel rotor field-oriented control to optimize unbalanced power operation. Jia et al. [11] studied the power flow control strategy of an FCV drivetrain based on the open-end winding motor, which represents a special type of dual winding motor. The space vector pulse-width modulation (SVPWM) method has been mainly researched to meet the demand for power sharing and balancing. In [12], the dual winding motor drive for the hybrid energy storage system (HESS) in an FCV was investigated, and the frequency dividing coordinated control and harmonic suppression method were established to enhance the power distribution performance under unbalanced winding power operating conditions. Krzysztof [13] investigated the indirect field-oriented control (IFOC), direct field-oriented control (DFOC), and direct torque control method for the DWM in detail. The result indicated that, from the control point of view, the DWM could be considered as one six-phase motor or two three-phase motors with a shared rotor. Kali et al. [14] developed a robust discrete-time sliding mode control method combined with the time delay estimation for the inner current control loop of an IFOC of a six-phase motor drive. Li et al. [15] revealed the coupling effect between the direct axis ( $d$ -axis) and quadrature axis ( $q$ -axis), and a decoupling method was introduced to realize fast current control on each of the axes. Eswar et al. [16] designed a modified predictive torque control for an open-end winding induction motor by replacing the flux control with an equivalent reactive torque control to satisfy the torque and flux control objectives of the same units for achieving an improved control response. In addition to the system modeling, the coupling cancellation control and faulty operation of a DWM have been widely investigated [17–19]. However, the control systems and methods proposed

in the previous studies have not considered the current variation principle of a fuel cell because the main DC–DC converter has been eliminated.

### 1.5. Contributions and Organization

To achieve optimal active control of the input current of the DC link of a PEMFC under dynamic conditions of a vehicle, this paper proposes a steady-state power control method based on the boost charging of a dual-winding motor. This is an important and meaningful research goal for improving the durability of fuel cells, but it has not been addressed in the previous research work. Due to the consideration of the current characteristics of a fuel cell, the proposed dual-winding motor can work in the single-winding boost single-winding drive mode and realize the fuel cell power steady-state by boosting the fuel cell side to charge the power battery. The control solves the problem of low energy exchange efficiency between the dual power sources in the low-speed state and realizes a high-efficiency energy exchange in the full-speed state.

When an FCV runs at a low speed, the current dual-winding motor architecture can realize energy exchange between the two power sources through torque coupling, but since the motor runs away from the rated operating point at a low speed, the efficiency of the fuel cell charging the secondary battery will be low or the charging process will even be unable to complete. However, the proposed dual-source motor architecture can work in the single-winding step-up single-winding drive mode. When the motor runs in the low-speed range, the fuel cell side winding is used as a step-up inductor to charge the power battery without additional inductors, and the power battery side winding works as a conventional stator winding drive motor. When the motor runs in the high-speed range, the dual winding drive mode is adopted to ensure efficient energy exchange between the two power sources within the full speed range of the motor.

The rest of this paper is organized as follows: Section 2 introduces the working mode and basic framework of the proposed dual-winding motor system and provides a brief comparison and analysis of the proposed architecture and the traditional DC–DC architecture. Section 3 analyzes the PEMFC model and the boost model based on the proposed dual-winding motor architecture. Section 4 studies the circulating current problem between the three-phase windings on the boost side of the proposed architecture and proposes the Bang-Bang-PI control algorithm with a relatively fixed reference value to solve this problem and reduce energy consumption, which is beneficial to the fuel cell steady-state control. Section 5 analyzes and discusses the steady-state control effect of the fuel cell based on the proposed dual-winding motor architecture to verify the feasibility and effectiveness of the proposed scheme. Finally, Section 6 summarizes the paper.

## 2. System Architecture

### 2.1. Drivetrain Operation Modes

The operation modes can be categorized into three types: single-source mode, dual-source mode, and energy regulation mode, as shown in Table 1. In Table 1, O stands for releasing energy and I stands for absorbing energy. In the single-source and dual-source modes, no energy is internally transferred between the two windings. While in the energy transfer mode R1, the extra power of a PEMFC will charge the battery when the SOC is low under both traction and braking conditions.

### 2.2. System Framework

The comparison of the conventional and DWM-based drivetrain topologies of an FCV is shown in Figure 1. In the conventional drivetrain topology, a DC–DC converter is used to provide power sharing and voltage adapter, which can be realized by regulating the output voltage of the DC–DC converter [20]. At the same time, a higher carrier frequency of the DC–DC converter increases the degree of electromagnetic interference. In contrast, in the DWM-based topology, energy exchange can be realized at low speed without additional chokes.

Table 1. Operation modes of the drivetrain.

| Operation Mode       | Sub-Mode | PEMFC | Battery | Motor | Vehicle           |
|----------------------|----------|-------|---------|-------|-------------------|
| Single-source mode   | S1       | Null  | O       | I     | Traction          |
|                      | S2       | Null  | I       | O     | Braking           |
| Dual-source mode     | D1       | O     | O       | I     | Boost traction    |
| Energy transfer mode | R1       | O     | I       | I     | Charging-traction |
|                      | R2       | O     | I       | O     | Charging-braking  |

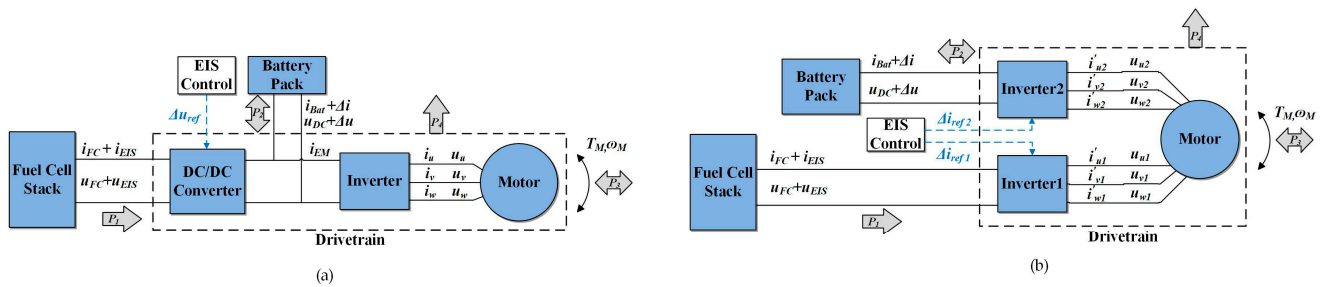


Figure 1. Framework and power flow of the FCV drivetrain: (a) Conventional topology; (b) DWM-based topology.

The DWM has two sets of three-phase windings and a shared rotor, which constitutes an electromechanical system with three energy ports. The DWM is powered by two inverters with reduced ratings fed by two power sources, a fuel cell stack, and a battery pack, so the main DC–DC converter used in the conventional drivetrain is eliminated. The energy flow between the three ports can be adjusted by controlling the two winding sets synergistically [21]. Sudden changes in the output current can cause variation in the water and gas content inside a PEMFC, which represents the driving force for extensive lifespan degradation. As a result, the PEMFC will provide the steady-state and unidirectional current, while the battery will output or absorb the transient power, thus acting as an energy buffer. Therefore, the boost circuit is drawn from the neutral point of the three-phase winding on the fuel cell side, so the extra energy of the PEMFC is charged to the power battery in the R1 energy transfer mode, realizing the steady-state power control of the PEMFC. The schematic of the DWM-based drivetrain is illustrated in Figure 2, where  $L_m$  denotes the filter inductor, which can stabilize the output current ripple of the fuel cell to a certain extent.

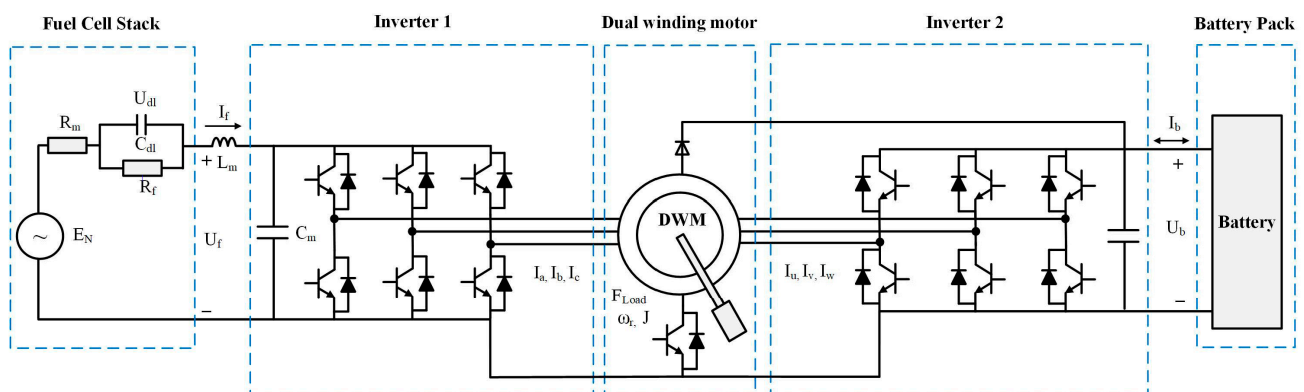


Figure 2. Schematic of the DWM-based drivetrain of an FCV.

### 3. Modeling

#### 3.1. PEMFC Model

##### 3.1.1. PEMFC Optimal Current Characteristics

Sudden changes and periodic ripples of the current load are two important affecting factors of PEMFC durability. Sudden changes in the electric load when a vehicle is accelerated or decelerated can cause variations in the water and gas content inside the fuel cell, which represents the driving force for extensive degradation processes. Hsu et al. [22] investigated the voltage undershoot phenomenon under the current-density step increase condition and found that undershoot amplitude became significant when the step was large, and the voltage recovery time became longer as the catalyst layer aged. The main reason for these results was that the mass flow controller could not supply enough hydrogen stoichiometry in the fast-changing operation mode because the gas response rate was much slower than the electrical load response. This transient operation could result in oxidant starvation, which could further affect the PEMFC durability. Furthermore, Yan et al. [23] performed the experimental test in situ to investigate the voltage undershoot at a fixed step (from zero to 500 mA/cm<sup>2</sup>) and a constant airflow rate (stoichiometry of two) for different loading rates from 0.1 s to 10 s. The results showed that when the loading rate was slow enough (e.g., 10 s), the undershoot phenomenon was slight and thus did not affect the durability of a fuel cell. Kim et al. [24] investigated the transient current response of the PEMFC under the 0.2-V/s voltage change rate under three different operating conditions: normal, starved, and excess stoichiometry. The experimental results showed that the overshoot and undershoot behaviors were observed under starved conditions. The overshoot behavior can be explained by the additional hydrogen consumption, non-uniform hydrogen-controlled current density, and sufficient consumption of hydrogen to draw ambient air into the flow field at the exit of the cell. The overshoot phenomenon can lead to the degradation of the proton exchange membrane. In addition, the current ripple can also affect PEMFC durability. Gemmen et al. [4] revealed that to ensure a negligible ripple effect, the current ripple frequency should be higher than 120 Hz, or the ripple should be less than 4% of the instantaneous theoretical current.

In summary, the optimal control of the DWM system should satisfy the following requirements:

- The DC current control for the PEMFC DC-link should be realized;
- The change rate of the current load should be controllable and as slow as possible (e.g., 10 s);
- Low-frequency current ripple (e.g., below 120 Hz) and large current ripple shall be avoided.

Knowing the dynamic property of PEMFC can help to establish a suitable control system for the drivetrain.

##### 3.1.2. PEMFC Stack Model

This model is mainly used to describe the current and voltage behaviors under dynamic load and their impacts on the DWM control system. The internal condition variations of the fuel cells will not be discussed in this study to avoid diverting the focus of this paper.

The cell voltage is evaluated using the Nernst equation, which provides the ideal cell voltage. The general expression is given by Equation (1), and for a certain type used in this paper, it is given by Equation (2).

$$E_{cell} = \frac{\Delta G}{2F} + \frac{\Delta S}{2F} (T - T_{ref}) + \frac{RT}{2F} \ln(P_{H_2} \cdot P_{O_2}^{0.5}) \quad (1)$$

$$E_{cell} = 1.29 - 8.45e^{-4}(T - 273.15) + 4.31e^{-4} \cdot T \cdot \ln(P_{H_2} \cdot P_{O_2}^{0.5}) \quad (2)$$

In Equations (1) and (2),  $\Delta G$  denotes the change in the free Gibbs energy,  $F$  is the Faraday constant,  $\Delta S$  is the entropy change, and  $R$  is the gas constant;  $P_{H_2}$  is the partial pressure of hydrogen,  $P_{O_2}$  is the partial pressure of oxygen,  $T$  is the battery temperature,

and  $T_{ref}$  is the reference temperature. Ignoring the influences of temperature and partial pressure,  $E_{cell}$  is set to 1.2 V in this study for the purpose of simplification.

Considering the activation, ohmic, and concentration losses, the PEMFC stack voltage can be calculated by:

$$u_f = N \times (E_{cell} - V_{act} - V_{ohm} - V_{con})$$

$$= N \times \left[ E_{cell} - \left( \frac{R \cdot T}{2\alpha F} \right) \ln \left( \frac{i}{i_0} \right) - i \cdot R_m + \left( \frac{R \cdot T}{2F} \right) \ln \left( 1 - \frac{i}{i_{lim}} \right) \right], \quad (3)$$

where  $i$ ,  $i_0$ , and  $i_{lim}$  denote the current density, exchange current density, and limit current density, respectively;  $V_{act}$ ,  $V_{ohm}$ , and  $V_{con}$  denote the activation loss, ohmic loss, and concentration loss voltage, respectively;  $N$  is the number of fuel cells in series,  $R_m$  denotes the membrane resistance, and the constant  $\alpha$  is the charge transfer coefficient, set to 0.5. The current density  $i$  is given in  $\text{mA cm}^{-2}$ , and the area-specific resistance  $R_m$  should be given in  $\text{k}\Omega \text{ cm}^2$ .

### 3.2. Boost Principle and Model Based on DWM Architecture

The working principle of the boost based on the DWM architecture is presented in Figure 3. As shown in Figure 3, in the single-winding boost single-winding drive mode, three upper-arm transistors ( $Q_1$ ,  $Q_2$ , and  $Q_3$ ) of the fuel cell side inverter are all closed, while three lower-arm transistors ( $Q_4$ ,  $Q_5$ , and  $Q_6$ ) are all open. The inverter on the secondary battery side maintains the inverter function and controls the current so that the motor can run in the state of electric power generation at a zero speed. By controlling transistor  $Q_7$  to repeatedly switch between on and off states, the DC current flows through the winding on the fuel cell side, which works as a boost inductor. In addition, the composite magnetic field generated by the fuel cell side windings connected in a star shape is zero, so it will not affect the rotating magnetic field generated by the secondary battery side windings. Therefore, it is possible to charge the secondary battery from the fuel cell under the operating state of the motor based on the principle of the boost converter.

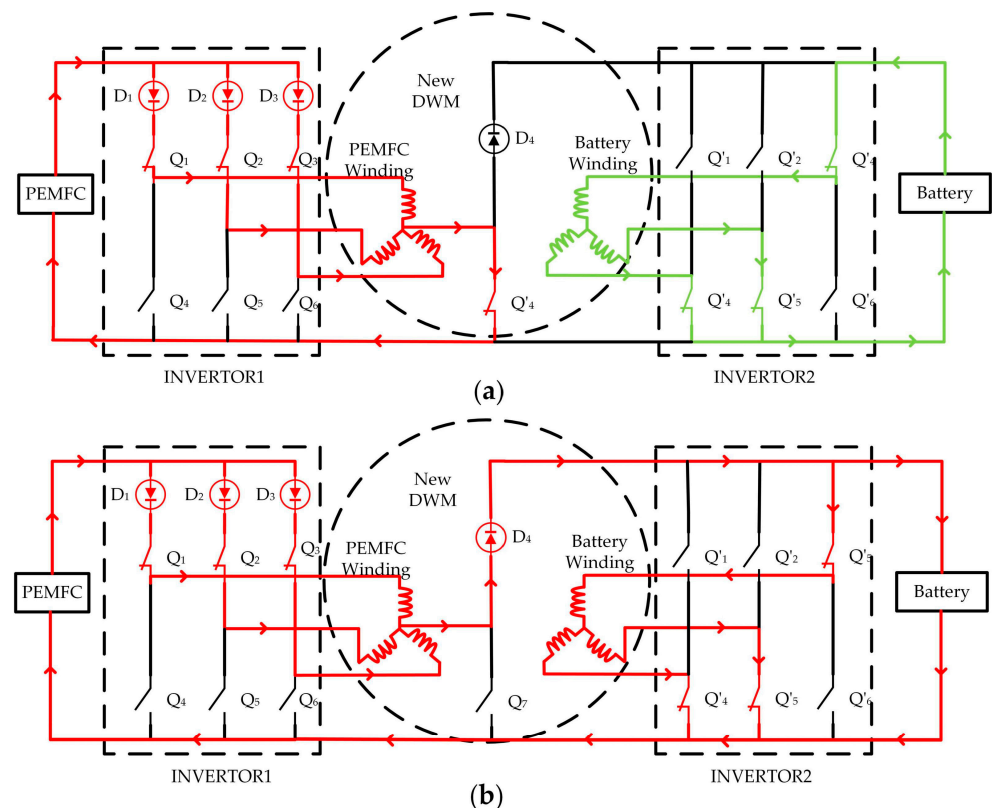


Figure 3. Boost schematic based on DWM architecture: (a) Energy storage stage; (b) Boost stage.

Considering that in the single-winding boost single-winding drive mode, the power battery side windings will generate an induced electromotive force with a phase difference of  $2 * \pi/3$  in each winding on the fuel cell side, which will lead to unbalanced currents in the three-phase windings and circulating currents. Further, this will produce additional reverse torque on the motor rotor, adversely affecting the stability of the motor and causing energy waste. Thus, a control algorithm needs to be adopted to adjust the duty cycle of the upper bridge IGBT ( $Q_1$ ,  $Q_2$ , and  $Q_3$ ) on the fuel cell side. Based on the basic principle of the boost circuit, the system boost ratio  $\varphi$  represents a function of the duty ratios  $Ton_1$ ,  $Ton_2$ ,  $Ton_3$ , and  $Ton_7$  of  $Q_1$ ,  $Q_2$ ,  $Q_3$  and  $Q_7$  and the output voltage  $U_f$  of the fuel cell, which can be expressed as follows:

$$\varphi = f(Ton_1, Ton_2, Ton_3, Ton_7, U_f). \quad (4)$$

#### 4. Control of Circulating Current between Windings

In the working state, there is a cross-coupling relationship between the two pairs of windings of the proposed DWM architecture. The driving-side winding generates an induced electromotive force with a phase difference of  $2 * \pi/3$  in the booster-side winding, which makes the phase current in the winding unable to balance. The generation of the induced current leads to excessive amplitude and high frequency of the bus current ripple, which affects the life of a fuel cell. This further results in a negative torque of the booster-side winding to the motor rotor, which affects motor stability. Therefore, the circulating current between the three-phase windings on the booster-side is the main problem to be solved in the single-winding boost single-winding drive mode of a DWM. The proposed DWM architecture has been rarely considered in the previous research, and the circulating current problem under this scheme has not been fully studied, so there has been no reliable solution developed yet.

The traditional boost converter control strategy mostly uses the closed-loop PI control combined with the synovial control algorithm, cooperative control algorithm, or other control algorithms. Its main advantage is that the system has good robustness and can greatly suppress the DC-current overshoot, but it often makes the system output voltage steady-state error large [25]. In addition, this type of control strategy is suitable only for the boost converter circuits with a single inductor but not for the boost system based on the proposed dual winding motor architecture.

##### 4.1. Control Principle

To solve the circulation problem, the instantaneous value of the current in the three-phase windings on the boost side should be equal, and the relationship between the three currents should meet the following requirement:

$$I_a = I_b = I_c = \frac{I_{dc}}{3}, \quad (5)$$

where  $I_a$ ,  $I_b$ , and  $I_c$  represent the current values of the three-phase windings and  $I_{dc}$  is the bus current.

The circulation problem caused by the proposed DWM configuration can greatly increase the control difficulty if the three-phase current in the boost side winding is coordinated to make it balanced, which will lead to poor system robustness and unsatisfactory control effect. Since the three control objects have the same control objectives, to simplify the control strategy, the three-phase current value should be controlled independently.

In view of the above discussion, this paper uses the Bang-Bang PI control algorithm to solve the circulating current problem between the three-phase windings on the boost side. The advantage of Bang-Bang control algorithm is that the response speed is fast, but the obvious disadvantage is that the steady-state error is large, which makes the current value fluctuate repeatedly up and down relative to the target value. The significant advantage of PI control is that the overshoot and steady-state error are extremely small, but with

a slow respond speed. Therefore, the two control methods have obvious complementary characteristics. In order to make the three-phase current quickly achieve equilibrium and stability, firstly, when the error value is large, the current value is quickly approximated by the current value by using the Bang-Bang control. When the error between the actual three-phase current value and the target value is less than a certain threshold, switch to PI control to make the three-phase current value accurately track the target current value. It is very important to determine the error threshold for switching control mode, which will directly affect the control effect and accuracy. Therefore, it needs to be revised through many experiments according to the requirements of control accuracy.

The schematic diagram of the designed Bang-Bang-PI controller is shown in Figure 4. In Bang-Bang-PI controller, the inversion threshold of selector block is 2. When the difference between  $I_{ref}$  and  $I_{real}$  is greater than 2 A, Bang-Bang control intervenes to reduce the error rapidly. When the error is greater than 2 A, PI control is involved to ensure a smaller steady-state error. The current of the three-phase winding on the boost side is taken as a control target, and the PWM duty ratio of the upper bridge wall IGBT in the inverter circuit on the boost side is taken as a control signal. The controller controls the opening and closing time of the upper bridge wall IGBT by outputting the PWM signals with different duty ratios so as to control  $I_a$ ,  $I_b$ , and  $I_c$  to make them equal. Thus, the PWM signal is adjusted according to the current error until the three-phase current reaches the current target value. The mathematical expression of the controller is shown in Equation (6):

$$|e| = |I_{ref} - I_j|, j = a, b, c;$$

$$u(t) = \begin{cases} \begin{cases} 1, e > 0 \\ 0, e \leq 0 \end{cases}, & |e| \geq 2; \\ k_p \cdot e + k_i \int_0^t edt, & |e| < 2. \end{cases} \quad (6)$$

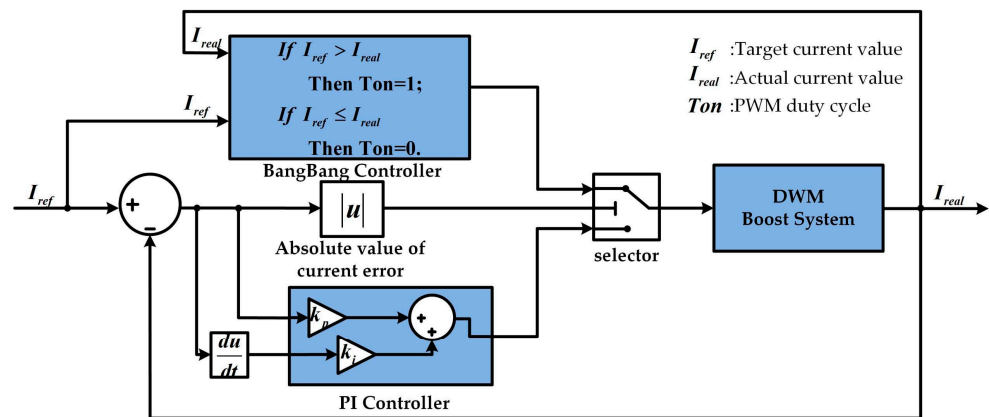


Figure 4. The Bang-Bang-PI controller.

## 4.2. Simulation Verification and Analysis

### 4.2.1. Construction of Simulation Platform

The simulation model of the proposed DWM architecture was established, and the simulation model of the current sharing control between three-phase windings on the boost side was based on the Bang-Bang-PI control, as shown in Figure 5. The input of the Bang-Bang-PI control system consisted of the currents  $I_a$ ,  $I_b$ , and  $I_c$  of the three-phase winding on the boost side, and the output included the duty cycles  $Ton_1$ ,  $Ton_2$ , and  $Ton_3$  of the PWM of the transistor on the upper bridge arm in the inverter circuit on the boost side. In addition, considering the actual load changes of the fuel cell vehicles and the charging characteristics of the power battery, the duty cycle  $Ton_7$  of transistor  $Q_7$  was adjusted and controlled in real-time according to the terminal voltage and charging current of the power battery to ensure the rationality and safety of power battery charging after the voltage

boost. It should be noted that simple PI control and other algorithms could be used to regulate  $T_{on7}$ . Therefore, this paper will not repeat it but briefly explain it for the purpose of demonstrating the rationality of the model.

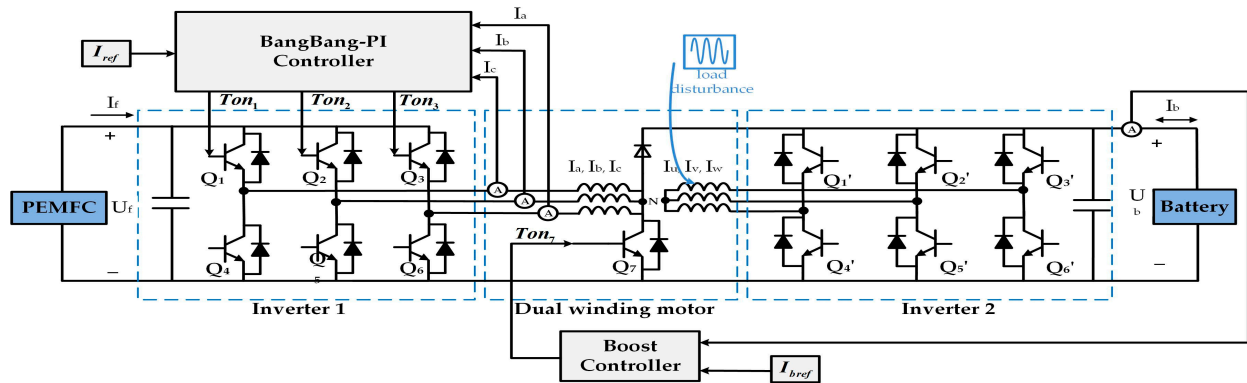


Figure 5. The current circulation control model used in the simulations.

#### 4.2.2. Simulation Results Analysis

The control effect of the Bang-Bang-PI system in solving the circulation problem between windings on the boost side of the proposed DWM architecture was verified by considering the actual load variation of fuel cell vehicles and the charging characteristics of power batteries. First, the current between the three-phase windings at the boost side and the current error between any two-phase windings under the control system without control (i.e., the transistor of the upper bridge arm at the boost side was set to the normally closed state) and under the Bang-Bang-PI control strategy were compared, as shown in Figure 6.

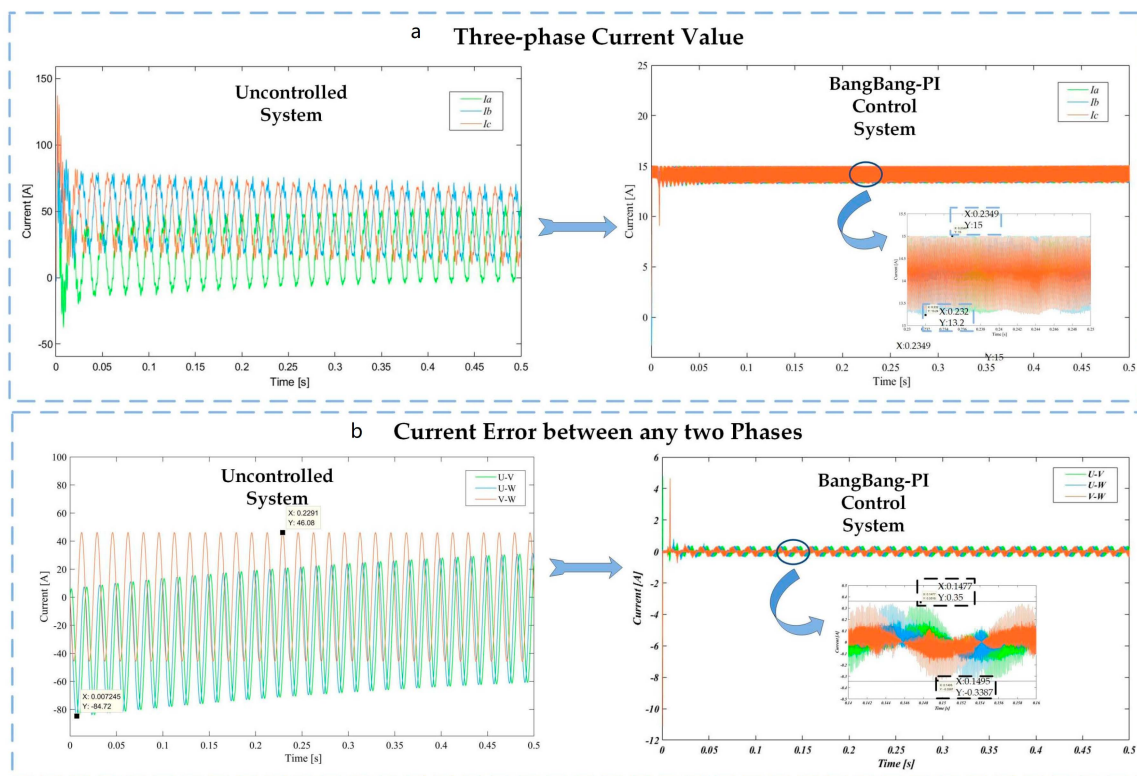


Figure 6. Comparison of three-phase current performance under different control modes: (a) Three-phase current value; (b) Current error between any two phases.

When the proposed DWM system was in the R1 energy transfer mode, the fuel cell side inverter circuit, and the three-phase winding were in the boost operation mode. As shown in Figure 6, when the PWM duty ratios  $Ton_1$ ,  $Ton_2$ , and  $Ton_3$  of the transistors  $Q_1$ ,  $Q_2$ , and  $Q_3$  of the upper bridge arm in the boost side inverter circuit were not controlled, the ripple amplitudes of currents  $I_a$ ,  $I_b$ , and  $I_c$  in the three-phase winding were large, which directly caused the DC ripple of the output current of the fuel cell to be much greater than 4%, thus affecting the service life of the fuel cell. In addition, the absolute value of the current difference between any two phases was as large as 80 A, and the current circulation problem was severe. This caused a large waste of energy, and the occurrence of circulation produced negative torque to the motor rotor, which had a great impact on the operation stability of the motor.

When the Bang-Bang-PI control strategy was used to control  $Ton_1$ ,  $Ton_2$ , and  $Ton_3$ , making them vary dynamically within the range of (0, 1) according to the work requirements. Compared with the case without control, the current value in the three-phase winding at the boost side was greatly reduced and stabilized within the range of (13.2, 15), and the DC ripple was small. The maximum absolute value of the current difference between any two phases was only 0.35 A. Thus, the circulation problem was effectively solved by the proposed control strategy, which is beneficial to the steady-state control of a fuel cell.

Under two working conditions, the values of  $I_a$ ,  $I_b$ , and  $I_c$  controlled by the Bang-Bang-PI control strategy were relatively small, which saved the energy. In addition, the duty cycle  $Ton_7$  could be adjusted to ensure the energy demand of the vehicle load and the safe charging demand of the power battery. Therefore, the proposed control strategy can not only solve the circulation problem but also save energy on the premise of ensuring the effect of pressure boost.

Based on the analysis results, the current reference value  $I_{ref}$  in the Bang-Bang-PI control system was set as a certain value according to the values of  $I_a$ ,  $I_b$ , and  $I_c$  without control, and its value was adjusted according to the requirements of practical application scenarios. The performances of the Bang-Bang-PI control system at different values are shown in Figure 7. As shown in Figure 7, under  $I_{ref}$  of 5 A, 10 A, and 15 A, the performance of the Bang-Bang-PI control system was good, so it could solve the circulation problem well, which proved the effectiveness of the proposed control method.

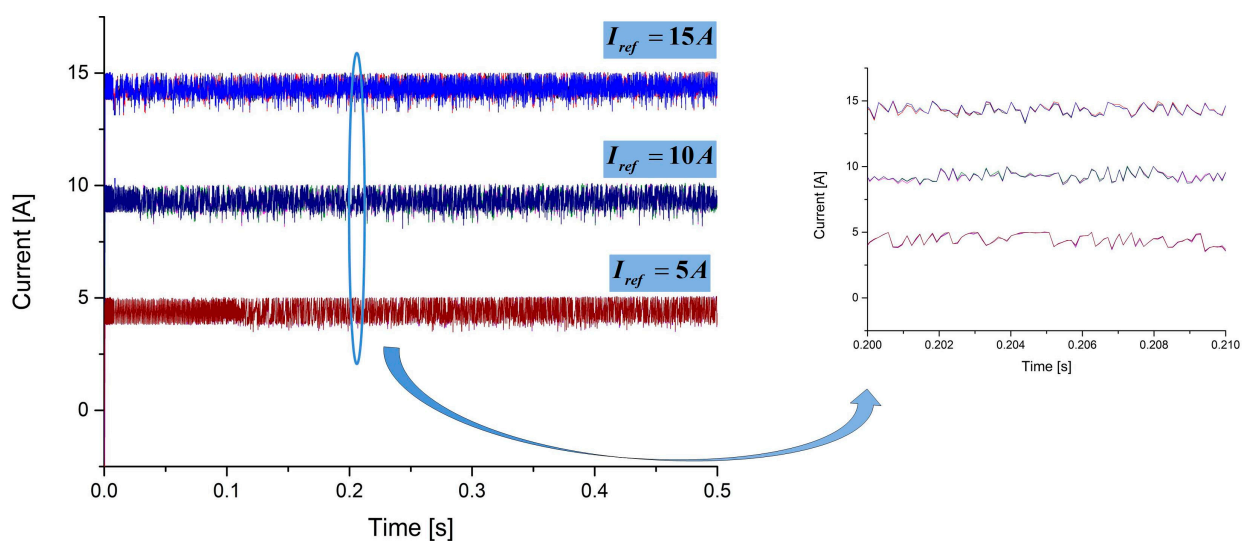


Figure 7. Three phase current values at different values of  $I_{ref}$ .

## 5. Results Analysis

First, the premise assumption of the simulation experiment was made: the SOC value of the power battery was less than 100%, and the value of 70% was taken in this study, so the power battery was in the rechargeable state by default.

The simulation parameters' values are given in Table 2.

**Table 2.** Simulation experiment parameters.

| Parameter Description and Its Mathematical Notation      | Value       |
|--|-------------|
| Operating voltage of a fuel cell stack, $U_f$            | 350 V       |
| Normal power of a fuel cell stack, $P_f$                 | 14 kW       |
| Operating voltage of a power battery, $U_b$              | 500 V       |
| Normal power of a power battery, $P_b$                   | 25 kW       |
| The state of charge (SOC) of the power battery, SOC      | 70%         |
| Inductance value of a phase winding, $L$                 | 1 mH        |
| Filter inductance value, $L_m$                           | 1 mH        |
| DC-Link value, $C_m$                                     | 400 $\mu$ F |
| Reference current of the step-up side winding, $I_{ref}$ | 15 A        |
| Proportional coefficient of the PI controller, $k_p$     | 0.85        |
| Integral coefficient of the PI controller, $k_i$         | 0.3         |
| Normal power of DWM, $P_m$                               | 48 kW       |
| Normal power of Inverter 1, $P_{v1}$                     | 18 kW       |
| Normal power of Inverter 2, $P_{v2}$                     | 30 kW       |
| Switching frequency of $Q_7$ , K                         | 10k Hz      |

Considering the load disturbance of an FCV and the charging demand of the power battery, taking the corresponding measures to solve the circulation problem in the boost side winding is the premise to ensure the steady-state of a PEMFC. To control the steady-state of a PEMFC, the PWM duty ratio of the bridge arm transistors  $Q_1$ ,  $Q_2$ , and  $Q_3$  in the boost side inverter circuit and the PWM duty ratio of transistor  $Q_7$  in the boost circuit were mixed controlled.

Based on the control mode proposed in this paper, the performance of the fuel cell output current is shown in Figure 8. Zhou et al. [23] studied the effect of the low-frequency narrow pulse current on the degradation of the proton exchange membrane fuel cells. Their results showed that the narrow pulse current of 4 ms did not affect the life of the fuel cell because there was no gas shortage, the changes in relative humidity and membrane moisture content were less than 1%, and the pressure difference varied within a specified range [26]. As shown in Figure 8, this study focused on the steady-state control system of the fuel cell under the proposed DWM architecture. On the premise of solving the circulation problem and considering the reasonability of voltage boost charging, the output narrow pulse current of the fuel cell in the boost mode was only 2.1 ms, so the fuel cell life was not affected. Second, in the initial stage of the voltage boost, the PWM duty cycle of the upper bridge arm IGBT was inconsistent due to the problem of circulation control between the three-phase windings. In the current decline stage, the current had decayed to zero before the next phase was triggered, so the current waveform was discontinuous. However, since the current discontinuity lasted only for 5 ms, its effect on the system performance was negligible. In addition, taking the output current of the stabilization stage in the time range of (0.20 s, 0.22 s) as an example, the peak-peak value of the pulsation waveform was only 0.06 A (i.e., the ripple was only 0.16%, which was far less than 4% that represented the value under which the fuel cell life was not affected). Therefore, the fuel cell had excellent stability under the proposed pressure boost mode.

As shown in Figure 8c, in the time range of (0.008 s, 0.06 s), the output current ripple was large, having a certain overshoot, but it still had a fast dynamic response speed. Therefore, further analysis in the frequency domain after the fast Fourier transformation (FFT) of the output current in this time period was conducted to discuss its specific influence on the steady-state of the fuel cell. The spectrum diagram is shown in Figure 9. The study

of Gemmen revealed that the DC ripple of fuel cells should be avoided in the frequency range below 120 Hz. In this study, the proportion  $\rho$  in the frequency range of  $f_{th} = 120$  Hz was calculated by:

$$\rho = \frac{\sqrt{\sum_{n=0}^{N_{f_{th}}} i_n^2}}{\sqrt{\sum_{n=0}^{N_{f_{max}}} i_n^2}}, \quad (7)$$

where  $N_{f_{th}}$  denoted the number of FFT transformation points corresponding to  $f_{th}$ ,  $N_{f_{max}}$  was the number of points corresponding to the maximum frequency of the FFT transformation, and  $i_n$  was the current amplitude at the  $n$ th frequency point. The calculated value of  $\rho$  was 11%, i.e., the frequency range of  $(0, f_{th})$  within 52 ms accounted only for 11%, and its influence on the stability of the fuel cell was negligible.

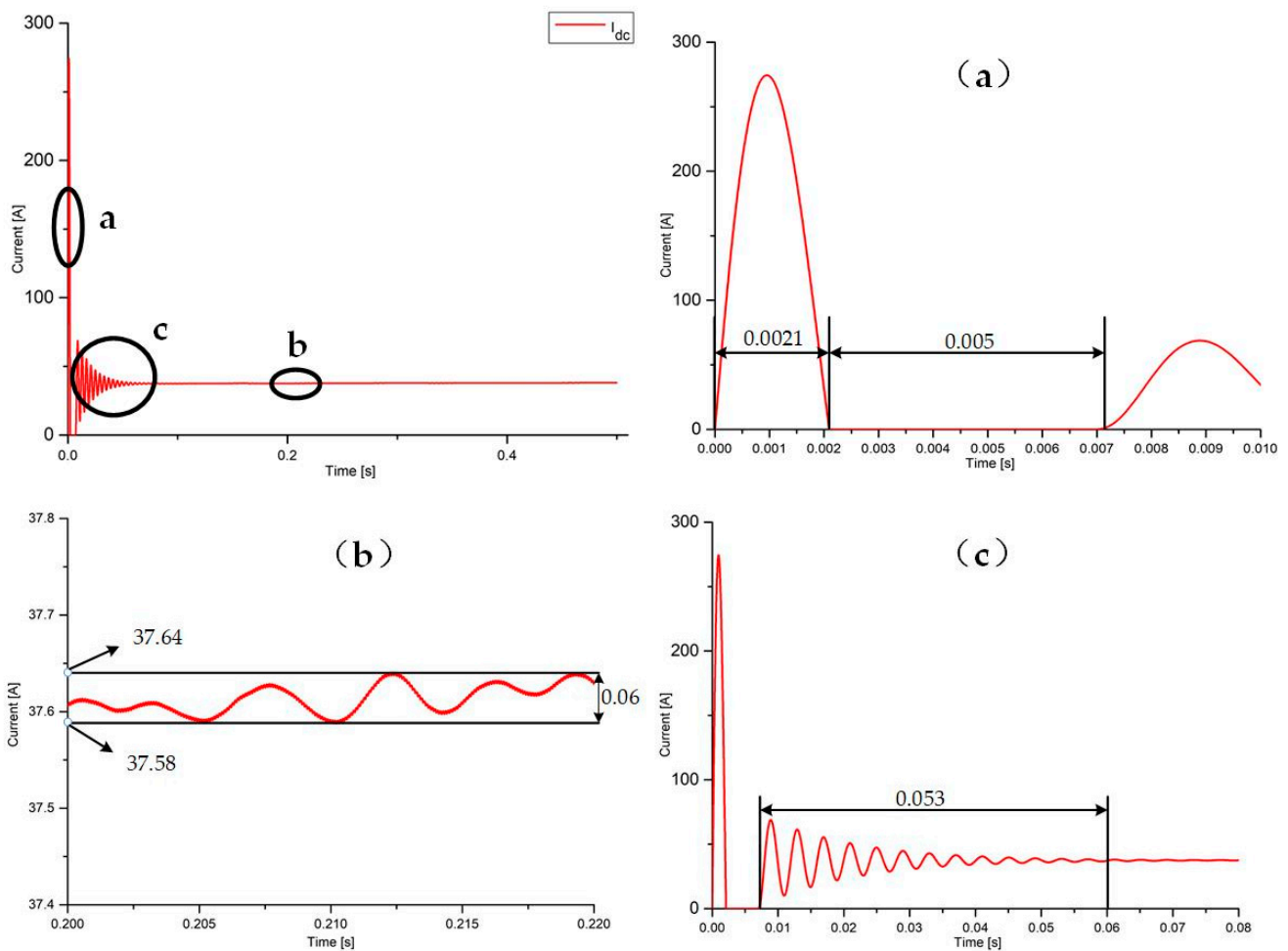


**Figure 8.** The fuel cell output current performance: (a) Narrow-pulse current and current discontinuous condition; (b) Current waveform at the steady-state; (c) Current waveform in the non-steady-state.

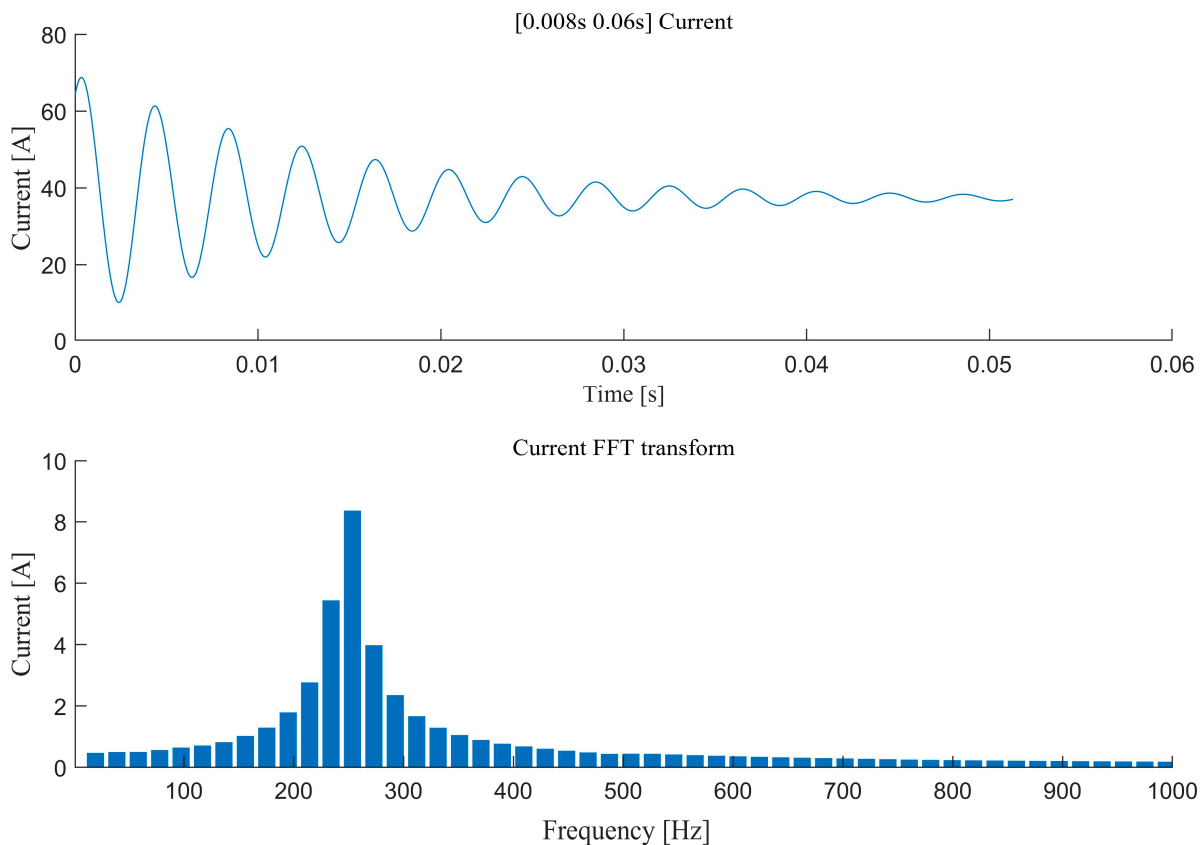


Figure 9. The current FFT analysis in the time range of (0.008 s, 0.06 s).

## 6. Conclusions

This paper studies one of the neglected topics in fuel cells-related literature based on a dual winding motor drive application. Based on the existing DWM drive system architecture, an innovative DWM-based topology, which combines the boost and inverter circuits to realize the steady-state control of a fuel cell, is proposed. The simulation results show that the proposed method is suitable for FCV applications based on dual winding motors and can achieve optimal and reliable control of the fuel cell stability. Thus, it represents a promising solution for the FCV driveline system and is of great significance for replacing the traditional high-cost DC–DC drive scheme.

In addition, a Bang-Bang-Pi control scheme with a fixed reference value is proposed to solve the problem of the current imbalance between three-phase windings. The proposed control scheme avoids the energy waste caused by circulation and prevents the negative torque generated by the step-up side winding to the motor rotor, which affects motor stability.

Finally, considering the reasonable feasibility of boost charging and solving the circulating current problem, the fuel cell outputs 2.1 ms of the narrow pulse current in the initial stage of the boost mode, and the intermittent current lasts only 5 ms. Under the stable condition, the current ripple is 0.16%, which is much smaller than the safety threshold of 4%, and the proportion of ripple frequency higher than 120 Hz in the unstable state is 89%. Therefore, the proposed architecture can realize the optimal steady-state control of a fuel cell.

Although this work studies only the permanent magnet motor, the proposed method can be extended to the induction and open-winding motors. However, there are still many challenges and open issues in this research area. For instance, one of the open issues to be addressed is the interference of the boost side winding to the drive side winding in the boost mode. The model only analyzes and discusses the dual winding motor and energy source system, without considering the whole vehicle power transmission system, ignoring the energy loss and transmission efficiency in the process of mechanical transmission. In

addition, Li et al. [27] pointed that the oxygen reduction (ORR) is the key bottleneck in the performance of fuel cells, and identified two reasons why it is difficult to find transition metal oxides (TMOs) with a high ORR activity, which is also of great significance to realize the operation stability of fuel cells. With such knowledge, an improved dual winding motor drive technology could be possible, which could ensure the durability and cost necessary for achieving commercial success.

**Author Contributions:** Conceptualization, Y.Z., and C.C.; methodology, W.C., J.M. and C.C.; software, W.C. and C.C.; validation, C.C., Y.Z. and J.M.; formal analysis, W.C. and C.C.; writing—original draft preparation, W.C. and J.M.; writing—review and editing, C.C. and Y.Z.; supervision, Y.Z. All authors have read and agreed to the published version of the manuscript.

**Funding:** It is gratefully acknowledged that this work has been supported by the National Key R&D Program of China (2018YFE0105100).

**Institutional Review Board Statement:** Not applicable.

**Informed Consent Statement:** Not applicable.

**Data Availability Statement:** Not applicable.

**Conflicts of Interest:** The authors declare no conflict of interest.

## References

1. Thounthong, P.; Chunkag, V.; Sethakul, P. Comparative study of fuel-cell vehicle hybridization with battery or supercapacitor storage device. *IEEE Trans. Veh. Technol.* **2009**, *58*, 3892–3904. [\[CrossRef\]](#)
2. Chen, H.; Pei, P.; Song, M. Lifetime prediction and the economic lifetime of Proton Exchange Membrane fuel cells. *Appl. Energy* **2015**, *142*, 154–163. [\[CrossRef\]](#)
3. Theiler, A.; Karpenko-Jereb, L. Modelling of the mechanical durability of constrained Nafion membrane under humidity cycling. *Int. J. Hydrogen Energy* **2015**, *40*, 9773–9782. [\[CrossRef\]](#)
4. Gemmen, R.S. Analysis for the Effect of Inverter Ripple Current on Fuel Cell Operating Condition. *J. Fluids Eng.* **2003**, *125*, 576–585. [\[CrossRef\]](#)
5. Daud, W.; Rosli, R.; Majlan, E.H.; Hamid, S.; Mohamed, R.; Husaini, T. PEM fuel cell system control: A review. *Renew. Energy* **2017**, *113*, 620–638. [\[CrossRef\]](#)
6. Holmes, D.G.; Lipo, T.A. *Pulse Width Modulation for Power Converters*; IEEE Press: Piscataway, NJ, USA, 2003.
7. McGrath, B.P.; Holmes, D.G. A general analytical method for calculating inverter dc-link current harmonics. *IEEE Trans. Ind. Appl.* **2017**, *45*, 1851–1859. [\[CrossRef\]](#)
8. Emadi, A.; Rajashekara, K.; Williamson, S.S.; Lukic, S. Topological Overview of Hybrid Electric and Fuel Cell Vehicular Power System Architectures and Configurations. *IEEE Trans. Veh. Technol.* **2005**, *54*, 763–770. [\[CrossRef\]](#)
9. Alberti, L.; Bianchi, N. Experimental Tests of Dual Three-Phase Induction Motor under Faulty Operating Condition. *IEEE Trans. Ind. Electron.* **2011**, *59*, 2041–2048. [\[CrossRef\]](#)
10. Bojoi, R.; Tenconi, A.; Farina, F. Dual-source fed multiphase induction motor drive for fuel cell vehicles: Topology and control. In Proceedings of the PESC, Recife, Brazil, 12–16 June 2005; pp. 2676–2683.
11. Jia, Y.F.; Xu, N.; Chu, L. Power flow control strategy based on the voltage vector distribution for a dual power electric vehicle with an open-end winding motor drive system. *IEEE Access* **2018**, *6*, 54910–54926. [\[CrossRef\]](#)
12. Hu, S.; Liang, Z.; Zhang, W.; He, X. Research on the Integration of Hybrid Energy Storage System and Dual Three-Phase PMSM Drive in EV. *IEEE Trans. Ind. Electron.* **2017**, *65*, 6602–6611. [\[CrossRef\]](#)
13. Pieńkowski. Analysis and control of dual stator winding induction motor. *Arch. Electr. Eng.* **2012**, *61*, 421–438. [\[CrossRef\]](#)
14. Kali, Y.; Ayala, M.; Rodas, J.; Saad, M.; Doval-Gandoy, J.; Gregor, R.; Benjelloun, K. Current Control of a Six-Phase Induction Machine Drive Based on Discrete-Time Sliding Mode with Time Delay Estimation. *Energies* **2019**, *12*, 170. [\[CrossRef\]](#)
15. Li, Y.; Hu, Y.W.; Huang, W.X. Decoupling control of the dual stator-winding induction generator using SVM. In Proceedings of the PESC, Rhodes, Greece, 15–19 June 2008; pp. 3366–3370.
16. Eswar, K.M.R.; Kumar, K.V.P.; Kumar, T.V. A simplified predictive torque control scheme for open-end winding induction motor drive. *IEEE J. Emerg. Sel. Top. Power Electron.* **2019**, *7*, 1162–1172. [\[CrossRef\]](#)
17. GSingh, G.K.; Nam, K.; Lim, S.K. A Simple Indirect Field-Oriented Control Scheme for Multiphase Induction Machine. *IEEE Trans. Ind. Electron.* **2005**, *52*, 1177–1184. [\[CrossRef\]](#)
18. Bojoi, R.; Tenconi, A.; Griva, G. Vector control of dual three phase induction-motor drives using two current sensors. *IEEE Trans. Ind. Appl.* **2006**, *42*, 1284–1292. [\[CrossRef\]](#)
19. Satake, A.; Okamoto, Y.; Kato, S. Design of Coupling Cancellation Control for a Double-winding PMSM. *IEEE J. Ind. Appl.* **2017**, *6*, 29–35. [\[CrossRef\]](#)

20. Geng, Z.; Hong, T.; Qi, K.; Ambrosio, J.; Gu, D. Modular Regenerative Emulation System for DC–DC Converters in Hybrid Fuel Cell Vehicle Applications. *IEEE Trans. Veh. Technol.* **2018**, *67*, 9233–9240. [[CrossRef](#)]
21. Ohto, Y.; Noguchi, T.; Sasaya, T. Space vector modulation of dual inverter with battery and capacitor across DC buses. In Proceedings of the PEDS, Honolulu, HI, USA, 12–15 December 2017; pp. 1172–1177.
22. Hsu, C.-Y.; Weng, F.-B.; Su, A.; Wang, C.-Y.; Hussaini, I.S.; Feng, T.-L. Transient phenomenon of step switching for current or voltage in PEMFC. *Renew. Energy* **2009**, *34*, 1979–1985. [[CrossRef](#)]
23. Yan, X.; Hou, M.; Sun, L.; Cheng, H.; Hong, Y.; Liang, D.; Shen, Q.; Ming, P.; Yi, B. The study on transient characteristic of proton exchange membrane fuel cell stack during dynamic loading. *J. Power Sources* **2007**, *163*, 966–970. [[CrossRef](#)]
24. Kim, S.; Shimpalee, S.; Van Zee, J.W. The effect of stoichiometry on dynamic behavior of a proton exchange membrane fuel cell (PEMFC) during load change. *J. Power Sources* **2004**, *135*, 110–121. [[CrossRef](#)]
25. Wu, Z.; Hao, Y. Bang Bang fuzzy PI control of wheel cylinder pressure in vehicle EHB system. *J. Mach. Des. Manuf.* **2021**, *1*, 188–192.
26. Zhou, Y.; Huang, L.; Sun, X. Impact of Low Frequency Narrow Pulse Current on the Degradation of Proton Exchange Membrane Fuel Cells. *J. Fuel Cells* **2019**, *19*, 561–569. [[CrossRef](#)]
27. Li, H.; Kelly, S.; Guevarra, D.; Wang, Z.; Wang, Y.; Haber, J.A.; Anand, M.; Gunasooriya, G.T.K.K.; Abraham, C.S.; Vijay, S.; et al. Analysis of the limitations in the oxygen reduction activity of transition metal oxide surfaces. *Nat. Catal.* **2021**, *4*, 463–468. [[CrossRef](#)]